Available online at www.sciencedirect.com
SCIENCE DIRECT
Thermochimica Acta 435 (2005) 213–221
thermochimica acta
www.elsevier.com/locate/tca

On the crystallization mechanism of ETS-10 titanosilicate synthesized in gels containing TAABr

C.C. Pavel [a,*], P. De Luca [b], N. Bilba [a], J. B.Nagy [c], A. Nastro [b]

[a] *Al. I. Cuza University of Iasi, Faculty of Chemistry, Department of Chemical Technology and Materials Chemistry, 11 Carol I Bd., 700506 Iasi, Romania*
[b] *University of Calabria, Dipartimento di Pianificazione Territoriale, 87036 Arcavacata di Rende (Cs), Italy*
[c] *Laboratoire de R. M. N., Faculté Universitaires N.D. de la Paix, Rue de Bruxelles 61, B-5000 Namur, Belgium*

Received 10 May 2004; received in revised form 11 April 2005; accepted 24 May 2005
Available online 11 July 2005

Abstract

Thermal analysis of the products resulted during crystallization of ETS-10 by using starting co gels with molar composition 5.0 Na_2O–3.0 KF–TiO_2–6.4 HCl–TAABr–7.45 SiO_2–197.5 H_2O, where tetralkylammonium (TAA) are tetramethyl (TMA), tetraethyl (TEA), tetrapropyl (TPA) and tetrabutylammonium (TBA), was performed. The effect of TAA^+ cations (ionic radius in hydrated forms, shapes and hydrophilic/hydrophobic character) on the crystallization of ETS-10 is evident from the induction time, t_i ($TMA^+ \ll TEA^+ < TPA^+ < TBA^+$), the rate of crystallization, R ($TMA^+ < TEA^+ < TPA^+ < TBA^+$), morphology and size of crystallites. Organic cations play a "pore filling" role rather than as a "structure-directing" agent. The relatively flexible molecules of the symmetric tetraalkylammonium cations mixed with alkali cations (Na^+, K^+) participate directly at prenucleation and nucleation steps by their interaction with the silicate and titanate in aqueous colloidal dispersion.

Keywords: Crystallization mechanism; Thermal analysis; TAA cations; ETS-10

1. Introduction

Zeolites are microporous crystalline hydrated aluminosilicates, with a rigid three-dimensional atomic structure, consisting of a network of interconnected tunnels and cages which are built from [SiO_4] and [AlO_4] tetrahedra [1–2]. Their uniform molecular size pores give to zeolites the capacity to separate mixtures of substances on the molecular level, which allows them to be termed molecular sieves. The main applications of zeolites in fields of commercial importance are as sorbents, ion exchangers, shape-selective catalysts or catalyst supports [3–7].

The structure and properties of the precise zeolite formed are highly dependent on the physical and chemical nature of the reactants used, their overall chemical composition, the type of templating cation (inorganic or/and organic) and the particular synthesis conditions used (temperature, time and pH). Therefore, zeolite researchers have not only developed novel structures and applications but also investigated the nucleation and crystal growth mechanism, ultimately aimed at their design for specific applications. Two theories have been proposed to explain the nucleation and growth of zeolite crystals [8]. In the solid–solid transformation mechanism (heterogeneous mechanism), crystallization of zeolite occurs directly by the reorganization of amorphous gel (hydrogel) to crystalline phase. In the solution crystallization mechanism (homogeneous mechanism) nuclei form and grow into crystals by incorporation of soluble species [9]. The gel dissolves continuously, and the dissolved species are transported to the nuclei crystals in the solution. It was emphasized that nucleation is closely related to the amorphous gel, whereas the crystal growth is related to solution by progressive incorporation of soluble species [10]. In addition to zeolite formation

* Corresponding author. Tel.: +40 232 201384; fax: +40 232 201313.
E-mail address: clpavel@uaic.ro (C.C. Pavel).

0040-6031/$ – see front matter © 2005 Elsevier B.V. All rights reserved.
doi:10.1016/j.tca.2005.05.022

via these two transformations, there is evidence to indicate that both transformations can sometimes occur simultaneously. In some cases, zeolites (A, L, MFI) can also be crystallized in a single-solution system containing no secondary solid gel phase [11]. From the single-phase solution studies, it appears that nucleation and subsequent crystallization can occur readily in the solution phase, leading to the possibility that the presence of a solid gel phase acts to supply nutrients to the solution only. The use of amines and quaternary ammonium cations in zeolite synthesis, developed by Barrer and Denny [12], has extended the number of zeolite structures discovered. The template theory states that various cations and amines can stabilize structural sub-units, thought to be precursors of crystalline zeolite species [13]. The true mechanism of the templating effect is still unclear. However, it is visualized that the zeolite structure grows around the cation of amine (usually referred to as a template), thus stabilizing certain pore structures [14].

The synthesis of ETS-10, a large pore titanosilicate molecular sieve with an ideal composition $(Na,K)_2Si_5TiO_{13}$, was first reported by Kuznicki [15]. The highly disordered structure can be considered as an intergrowth of two end member polymorphs (the chiral tetragonal polymorph A and the monoclinic polymorph B) [16–19]. In this structure, chains of $[TiO_6]$ octahedra are linked to two-folded chains of $[SiO_4]$ tetrahedra. The pore structure consists of 12, 7, 5 and 3 rings and has a dimensional wide pore channel system, whose minimum diameter is defined by 12-membered rings apertures (maximum aperture of 8 Å and micropore volume of 0.145 cm^3/g, respectively). ETS-10 has been synthesized under hydrothermal conditions (temperatures from ca. 180 to 250 °C, synthesis time from 16 h to 30 days, pH of initial gel in the range 10–12), without any organic template, using $TiCl_3$ [15–17,20–22], $TiCl_4$ [23–25], TiF_4 [22,26], TiO_2-anatas [20,22], TiO_2 nano-sized [22,27], $Ti_2(SO_4)_3$ [28], $(NH_4)_2TiF_6$ [22] as Ti sources and sodium silicate solution, fumed or colloidal silica as Si sources, in presence of NaOH, NaCl, KCl and KF. The crystallization field of ETS-10 depends on the quantities of Na_2O, K_2O, TiO_2 and SiO_2 in initial gel, Ti precursors, pH of synthesis gel, etc. ETS-10 is easily contaminated with quartz, titanosilicate ETS-4 or an unidentified phase [22,25,29,30].

ETS-10 has also been synthesized in the presence of organic template such as TMACl [31,32], pyrrolidine, TEACl, TPABr, 1,2-diamino-ethane [32], choline chloride and bromide salt of hexaethyldiquat-5 [33] and salts of tetralkylammonium and ethanolamine [34,35]. The effect of temperature (170, 190 and 210 °C) on the crystallization of ETS-10 and TAA-ETS-10 from starting co gels with molar composition $5.0Na_2O$–$3.0KF$–TiO_2–$6.4HCl$–$TAABr$–$7.45SiO_2$–$197.5H_2O$, crystallization curves, induction time (t_i), crystallization rate (R), Avrami–Erofeev parameters and apparent activation energy (E_a) were reported recently [35,51].

In this study we synthesized ETS-10 sample by hydrothermal method using gels of molar composition $5.0Na_2O$–$3.0KF$–TiO_2–$6.4HCl$–$TAABr$–$7.45SiO_2$–$197.5H_2O$ to investigate the role of the symmetric, partial flexible and hydrophilic/hydrophobic tetralkylammonium cations with different alkyl chain length on the evolution of crystallinity and morphology of crystals. DTG/TG analyses were used to obtain a quantitative distribution of TAA cations during the crystallization between liquid, gel and crystalline ETS-10.

2. Experimental

The titanosilicate TAA-ETS-10 synthesis was carried out according to the procedure described previously [35] from starting gels with molar composition $5.0Na_2O$–$3.0KF$–TiO_2–$6.4HCl$–$TAABr$–$7.45SiO_2$–$197.5H_2O$. The reaction mixtures were prepared by combining under stirring an acidic aqueous solution obtained by dissolving KF (40 wt.%, Panreac), $TiCl_4$ (50 wt.%, Merck), HCl (37 wt.%, Riedel de Haën) and distilled water with a basic aqueous solution obtained from sodium silicate solution (8 wt.% Na_2O, 27 wt.% SiO_2, 65 wt.% H_2O, Merck), NaOH solution (50 wt.%, Carlo Erba), an organic TAABr salt (Merck) and distilled water. The amorphous silica–titania gels were transferred into a PTFE-lined Morey type stainless steel autoclaves and heated at 190 ± 2 °C, under autogeneous pressure and under static conditions for a given period of time. After certain pre-set times, autoclaves were withdrawn from the oven and quenched with cold water. The solid products separated by centrifugation, washed with distilled water and dried at 100 °C overnight and the solid products obtained by the evaporation of the corresponding liquid phases and dried at 100 °C overnight were characterized by X-ray powder diffraction (Philips PW 1830 automated diffractometer, Cu Kα radiation), DTG/TG and DSC analyses (STA 429 Netzsch instrument) and ^{13}C NMR spectra (Bruker MSL 400 spectrometer).

3. Results and discussion

The XRD patterns of products synthesized without/with TAABr at 190 ± 2 °C for 72 h, shown in Fig. 1 are characteristic to ETS-10 [15,16,31], which belongs to two polymorphs one being tetragonal and other monoclinic.

In order to investigate the role of TAA^+ cations during ETS-10 crystallization, the crystallization kinetics were studied varying the synthesis time. The evolution of the crystallinity, calculated from XRD data are depicted in Fig. 2. The crystallinity of each sample was calculated by comparing the sum of intensity of three diffraction peaks at $2\theta = 5.95°$, 20.12° and 24.68° with that of a final crystalline sample (with the strongest XRD intensity) after removing the amorphous phase by an ultrasound technique [36].

Crystallization curves exhibit a typical sigmoid shape of process involving two stages, one is induction stage characterized by induction time (t_i) and the other is crystal growth

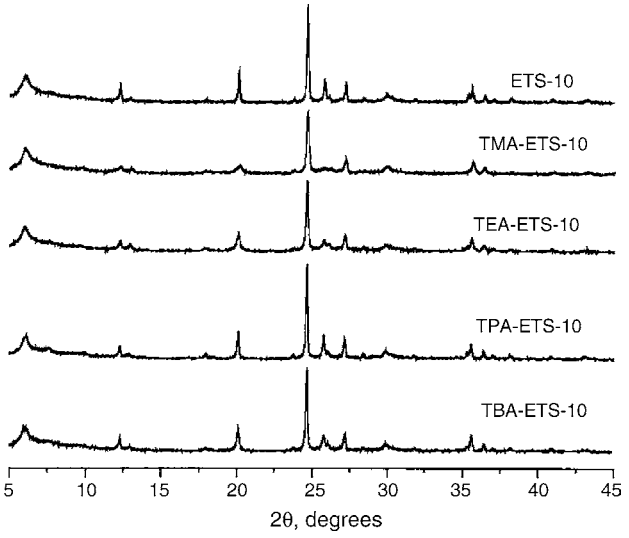

Fig. 1. XRD patterns of as-synthesized ETS-10 (no organic) and TAA-ETS-10 samples; 72 h, 190 ± 2 °C.

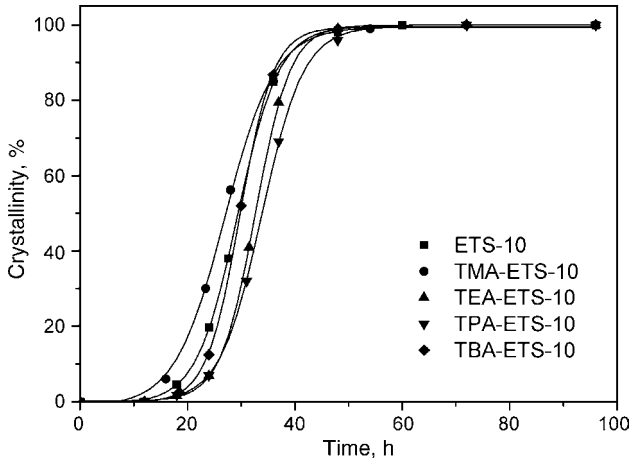

Fig. 2. Crystallization curves for ETS-10 (no organic) and TAA-ETS-10 sample from the synthesis system of $5.0Na_2O$–$3.0KF$–TiO_2–$6.4HCl$–TAABr–$7.45SiO_2$–$197.5H_2O$ at 190 ± 2 °C.

(slow and fast) characterized by rate of crystallization (R). Induction time (t_i) is an arbitrary point that corresponds to the time, in hours, for the appearance of 4% crystallinity. Rate of crystallization (R) expressed in $\%\,h^{-1}$ is computed from the crystallization curves as the steepest slope as a function of time. The data of t_i and R are listed in Table 1. The induction time (t_i) is slightly increased when TEA^+, TPA^+ and TBA^+ cations were used as the organic additives and is well decreased in the case of TMA^+ compared with no-organic ETS-10. The rate of nucleation during the zeolite crystallization, supposing the heat-up time eliminated and defined by the reciprocal of the induction time [37] varies in order: TMA-ETS-10 > no-organic ETS-10 > TBA-ETS-10 > TPA-ETS-10 > TEA-ETS-10. The rate of crystallization (R) increases in the following order: TMA-ETS-10 < TEA-ETS-10 < ETS-10 < TPA-ETS-10 < TBA-ETS-10.

Table 1
Induction time (t_i, h) and crystallization rate (R, $\%\,h^{-1}$) for the TAA-ETS-10 and ETS-10 crystallization at 190 ± °C

Parameters	Cations				
	No organic	TMA^+	TEA^+	TPA^+	TBA^+
t_i (h)	18.0	13.4	22.2	21.5	20.3
R ($\%\,h^{-1}$)	6.3	5.1	5.8	6.4	7.2

($5Na_2O$–$3.0KF$–TiO_2–$6.4HCl$–TAABr–$7.45SiO_2$–$197.5H_2O$), ($5Na_2O$–$3.0KF$–TiO_2–$6.4HCl$–$7.45SiO_2$–$197.5H_2O$).

The addition of a limited amount of TAABr salts in the initial co gel silica–titania composition influences the crystallization kinetics probably due to a modification of solubility of reactive species that affects nucleation and growth of crystals [38]. In aqueous solution, inorganic cations are known to play an important role on the ordering of water molecules [39,40]. The small cations (Na^+, Li^+, ...) which interact strongly with water molecules because of their high charge density breaking the original hydrogen bonds and organizing the water molecules around them in a water cluster are "structure-making" cations. The large cations (K^+, NH_4^+, Rb^+, ...) which interact with water molecules and break the original hydrogen bonds but the interaction is not strong enough to form an organized water cluster are "structure-breaking" cations. Presence of cations in liquid phase and in synthesis co gel affects the distribution of anionic species ranging from monomeric to oligomeric anions [38,41–43].

The TAA monovalent cations with different alkyl chain length easily deformable are at large cationic radii that form no strong hydrogen bond to water molecules in solutions. They are larger than alkali metal ions in unhydrated/hydrated form (Na^+ −0.95/3.58 Å; K^+ −1.33/3.31 Å; TMA^+ −2.79/3.67 Å; TEA^+ −3.37/4.00 Å; TPA^+ −3.79/

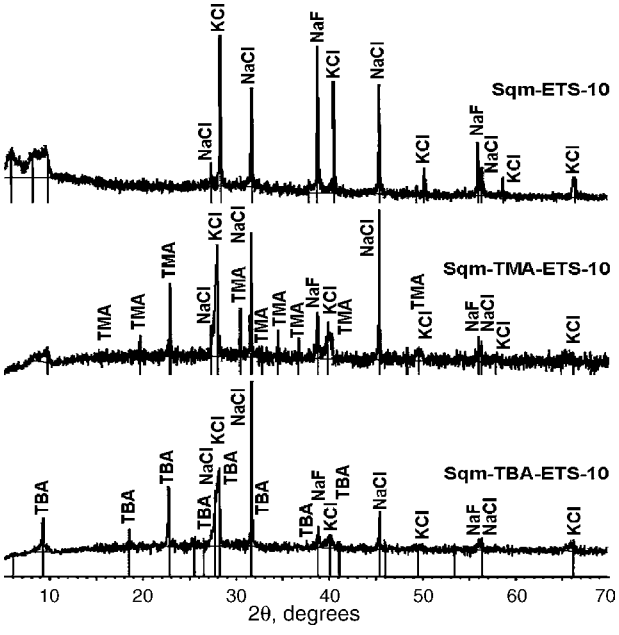

Fig. 3. XRD patterns of Sqm-ETS-10 (no organic) and Sqm-TAA-ETS-10 (TAA = TMA and TBA) solids from liquid phase of the synthesis system.

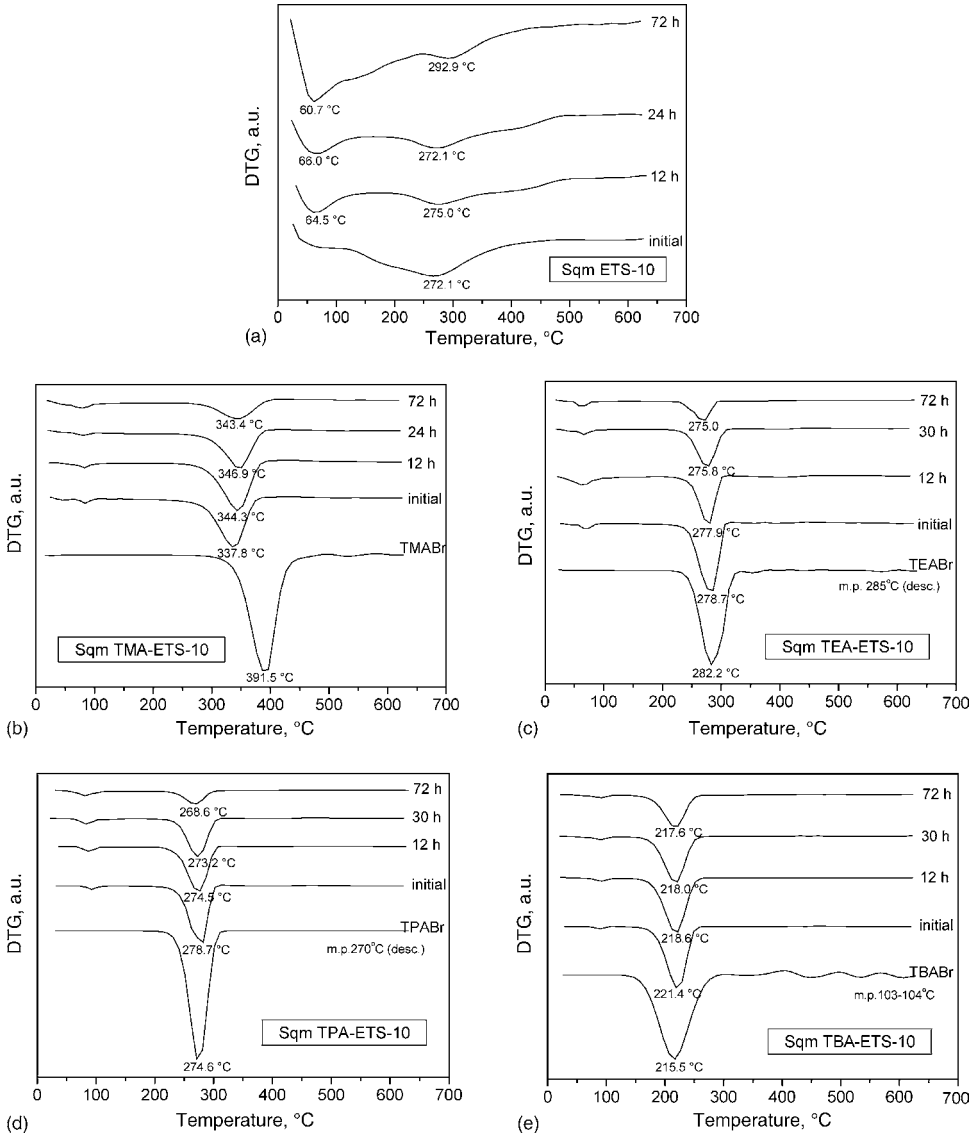

Fig. 4. DTG curves of Sqm-ETS-10 (no organic) and Sqm-TAA-ETS-10 solids (in comparison with pure TAABr salts); crystallization time, 0 (initial), 12, 24, 30 and 72 h at 190 ± 2 °C.

4.52 Å; TBA^+ −4.13/4.94 Å) [38,44–50] having a hydrophilic/hydrophobic character. The effect of TAA cations during the nucleation and crystals growth is attributed to "structure-breaking" effect on water or "hydrophobic interactions"; the concentration of bonded water rises with increasing TAA size and the cation–anion interactions are not so extensive.

The hydrophobic effect of TAA cations on the structuring of water increases with increasing cation size (TBA > TPA > TEA > TMA). A shorter alkyl chains of TMA^+ cations lead to more polar and relatively hydrophilic behavior, while TEA^+, TPA^+ and TBA^+ cations are increasing in hydrophobicity and TPA^+ and TBA^+ can make self-association in aqueous solution [47].

The faster induction time (h) was obtained during the crystallization of ETS-10 from co gel with molar ratio $5.0Na_2O$–$3.0KF$–TiO_2–$6.4HCl$–TAABr–$7.45SiO_2$–$197.5H_2O$ at 190 ± 2 °C for 72 h, in presence of TMA^+ cations (Table 1; Fig. 2), which is in a good agreement with reported data [29,31,34]. A source of TMA^+ cations could be TMABr [34], TMACl [22,26,31–33] or TMAOH. The presence of TEA^+, TPA^+ or TBA^+ instead of TMA^+ has a retarding effect towards nucleation time and crystallization rate compared with ETS-10 synthesis without organic molecules. Strongly hydrophobic TBA^+ ions have the lowest affinity to water. The smallest TMA^+ hydrated cations whose diameter is of ∼7.34 Å can be accommodated in the channels of ETS-10 whose maximum diameter is ∼8 Å.

The distribution of TAABr between liquid phase and solid phase during the crystallization process of ETS-10 was established by TG–DTG–DSC studies. The liquid phases, separated by centrifugation after 12, 24, 30 and 72 h of crystallization at 190 ± 2 °C, in equilibrium with solid phase (initially non-crystalline, mixture and finally-crystalline) after

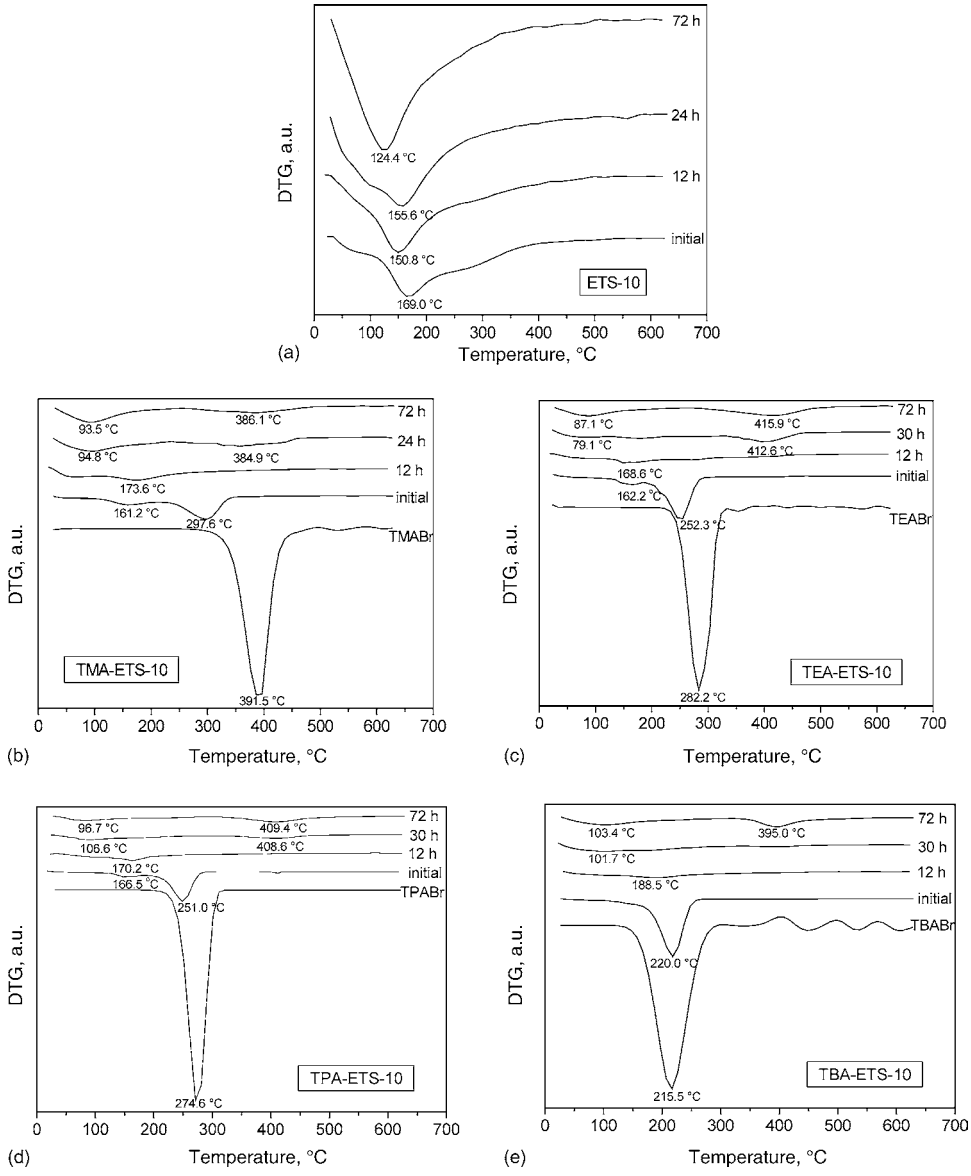

Fig. 5. DTG curves of ETS-10 (no organic) and TAA-ETS-10 solids; crystallization time, 0 (initial), 12, 24, 30 and 72 h at 190 ± 2 °C.

evaporation and drying gave the solids named Sqm-ETS-10 (without organic) and Sqm-TAA-ETS-10 (TAA being TMA, TEA, TPA and TBA). By initial time we designate the solids obtained soon after their preparation from gel and liquid after drying at 100 °C. The XRD data of Sqm-ETS-10 solid show the presence of NaCl, KCl and NaF (Fig. 3). The XRD data of Sqm-TAA-ETS-10 solids show the presence of TAA salts and of NaCl, KCl and NaF, respectively (Fig. 3). A small quantity of co gel silica–titania is indicated by the broadened peak between 9–10° and 2θ.

DTG curves of these solids are given in Fig. 4. One may see that in all Sqm-ETS-10 samples (Fig. 4a) are present two DTG peaks attributed to the elimination of water in two steps: the physiadsorbed water and hydrated water of Na^+ and K^+. Instead, in Sqm-TAA-ETS-10 samples, besides water peak the most important DTG peak corresponds to the elimination of organic TAABr salts in agreement with characteristic peaks of pure TAABr (Fig. 4 b-TMA, c-TEA, d-TPA, e-TBA).

The amount of TAABr decreases slowly with increase of crystallization time, but after 72 h, when crystalline ETS-10 is present, the content of TAABr is increased suggesting that TAA cations are progressively entrapped in ETS-10 structure as filling molecules. Maximum temperatures for the elimination of TEA, TPA and TBA from Sqm-TAA-ETS-10 (Fig. 4c–e) samples are close to that of pure TAABr salts, except the Sqm-TMA-ETS-10 sample where the elimination of TMA takes place at a lower temperature (337.8–346.9 °C) than of pure TMABr (391.5 °C) probably because TMA cation are hydrated.

TG data of Sqm-ETS-10 and Sqm-TAA-ETS-10 are listed in Table 2. The values of losses show that all Sqm-TAA-ETS-10 samples contain water and organic molecules and

Table 2
TG data of the Sqm-ETS-10 and of Sqm-TAA-ETS-10 solids (100 °C, 24 h)

Sample	Reaction time at 190 °C (h)	H_2O (wt.%)	TAA^+ cations (wt.%)	Total loss (wt.%)
Sqm-ETS-10	0	4.96	–	4.96
	12	6.42	–	6.42
	24	7.42	–	7.42
	72	12.28	–	12.28
Sqm-TMA-ETS-10	0	2.15	16.53	18.68
	12	2.38	15.50	17.88
	24	3.10	13.63	16.73
	72	5.55	8.53	14.08
Sqm-TEA-ETS-10	0	1.75	22.63	24.38
	12	2.53	17.59	20.12
	30	3.47	14.11	17.58
	72	3.40	8.03	11.43
Sqm-TPA-ETS-10	0	0.92	31.49	32.41
	12	1.26	28.64	29.90
	30	2.42	24.50	26.92
	72	3.89	10.26	14.14
Sqm-TBA-ETS-10	0	0.35	33.70	33.34
	12	1.01	32.09	33.10
	30	1.68	26.66	28.34
	72	1.87	20.08	21.95

Sqm-ETS-10 sample only water. In the case of Sqm-TAA-ETS-10 solids the loss of water increases and the loss of TAA^+ cations decreases with increasing reaction time from start to 72 h. The decreasing organic content is important after 24–30 h of reaction at 190 ± 2 °C when crystallinity of TAA-ETS-10 becomes 30–55% and 100% after 72 h. During the crystallization stage TAA cations transit from the liquid phase into solid amorphous phase and finally are entrapped in the ETS-10 structure as filling molecules. The temperature of the maximum elimination of organic cations decreases from TMA (343.4 °C, 72 h) to TBA (217.6 °C, 72 h) following the melting points, TMABr (>300 °C) and TBABr (103–104 °C).

The solid phases (initially non-crystalline mixture and finally-crystalline) obtained after separation of liquid phases at the prefixed reaction time (0, 24, 30 and 72 h) were named ETS-10 (without organic) and TAA-ETS-10 (in presence of TMA, TEA, TPA and TBA bromide). The DTG curves are shown in Fig. 5 and TG data are presented in Table 3.

In the ETS-10 samples (Fig. 5a) only one peak is observed corresponding to the loss of water from initial co gel (169.0 °C) and from zeolite channels (121.0 °C). In TAA-ETS-10 samples (Fig. 5 b–e) the TAA^+ cations are moving from co gel (initial) to liquid phase (after 12 h) but once the crystallization was complete (72 h) the TAA^+ cations are present in zeolite channels and their elimination takes place at higher temperatures compared with temperatures for pure TAABr. Because of the high loss peaks of pure TAABr, the quantity of TAA-ETS-10 samples taken for TG and DTG analysis were smallish, the peaks of water and TAA loss are small and broadened. The TG and DTG curves only of ETS-10 and TAA-ETS-10 with 100% crystallinity obtained at 190 ± 2 °C for 72 h are presented in Fig. 6 (heating rate of 10 °C min^{-1} in static air).

From Table 3 it can be seen that after 12 h of hydrothermal synthesis, all samples are still amorphous and the organic molecules are null. After 72 h, when the crystallinity of samples is 100%, the organic molecules are present in

Table 3
TG data of the ETS-10 and TAA-ETS-10 samples synthesized at 190 ± 2 °C for various times

Sample	Time (h)	Crystallinity (%)	H_2O (wt.%)	TAA^+ cations		Total loss (wt.%)
				wt.%	Mol%	
ETS-10	0	0	6.55	–	–	6.55
	12	0	8.15	–	–	8.15
	24	20	11.54	–	–	11.54
	72	100	13.23	–	–	13.23
TMA-ETS-10	0	0	4.63	7.85	0.131	12.47
	12	0	11.22	0	0	11.22
	24	35	9.53	4.17	0.069	13.71
	72	100	8.42	5.36	0.089	13.78
TEA-ETS-10	0	0	3.15	11.08	0.095	14.23
	12	0	10.67	0	0	10.67
	30	35	8.59	2.49	0.021	11.18
	72	100	6.74	6.97	0.059	13.71
TPA-ETS-10	0	0	3.18	13.41	0.078	16.59
	12	0	10.89	0	0	10.89
	30	30	8.88	4.62	0.027	13.50
	72	100	6.87	6.78	0.040	13.65
TBA-ETS-10	0	0	2.06	19.03	0.083	21.10
	12	0	8.47	0	0	8.47
	30	55	9.63	2.02	0.008	11.65
	72	100	8.27	5.31	0.023	13.58

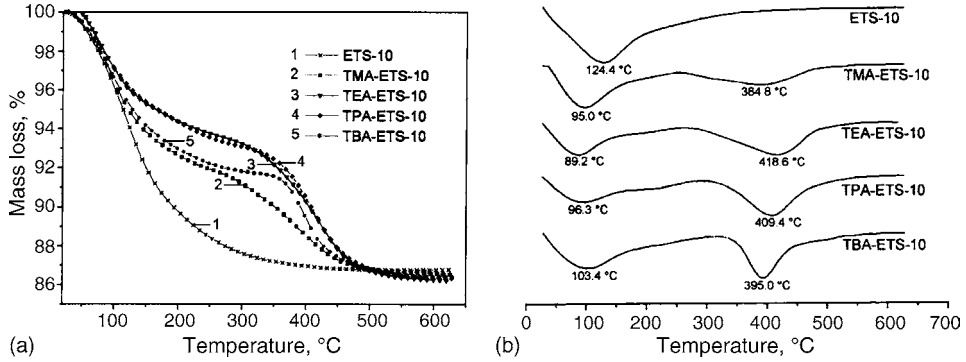

Fig. 6. TG (a) and DTG (b) curves of ETS-10 (no organic) and TAA-ETS-10; reaction time 72 h at 190 ± 2 °C, 100% crystallinity.

the microporous structure of ETS-10 together with water molecules. The water content decreases from ETS-10 to TAA-ETS-10. In TMA-ETS-10 case, the content of water is high (8.42 wt.%) because TMA^+ cations have small size and are in hydrated form. The water content decreases when TEA^+ (6.74 wt.%) and TPA^+ (6.87 wt.%) cations are incorporated in the structure and, finally, in TBA-ETS-10 case the water content increases (8.27 wt.%) because of the big size

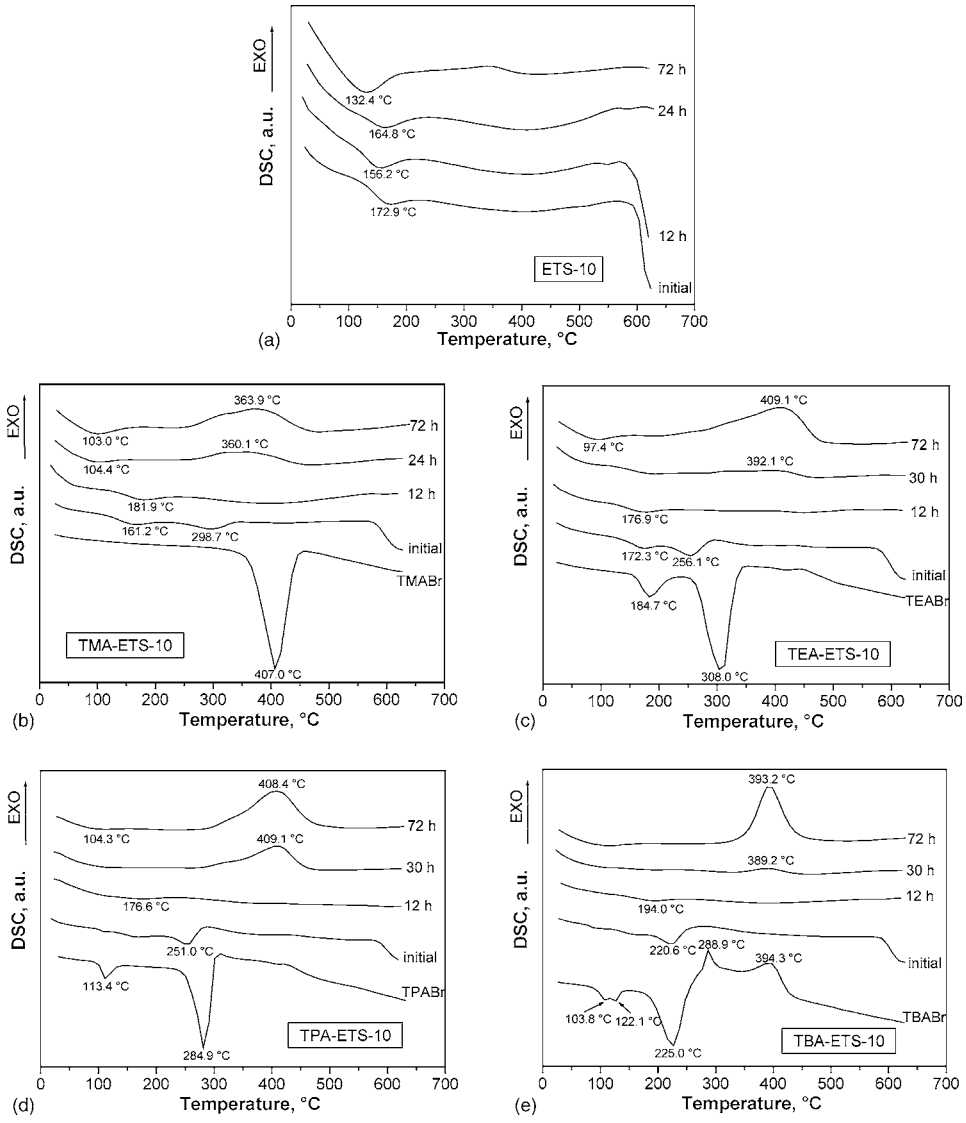

Fig. 7. DSC curves of ETS-10 (no organic) and TAA-ETS-10 solids separated after 0 (initial), 12, 24, 30 and 72 h reaction time at 190 ± 2 °C.

and hydrophobicity of TBA^+. The presence of TAA cations has an influence on both size (increase) and shape of crystals (from aggregate quasi-cubic to a thick plate-like and a bipyramidal with round edges) [31,33,35,51].

DSC curves of ETS-10 and TAA-ETS-10 solids, resulted after a prefixed time of crystallization, are given in Fig. 7.

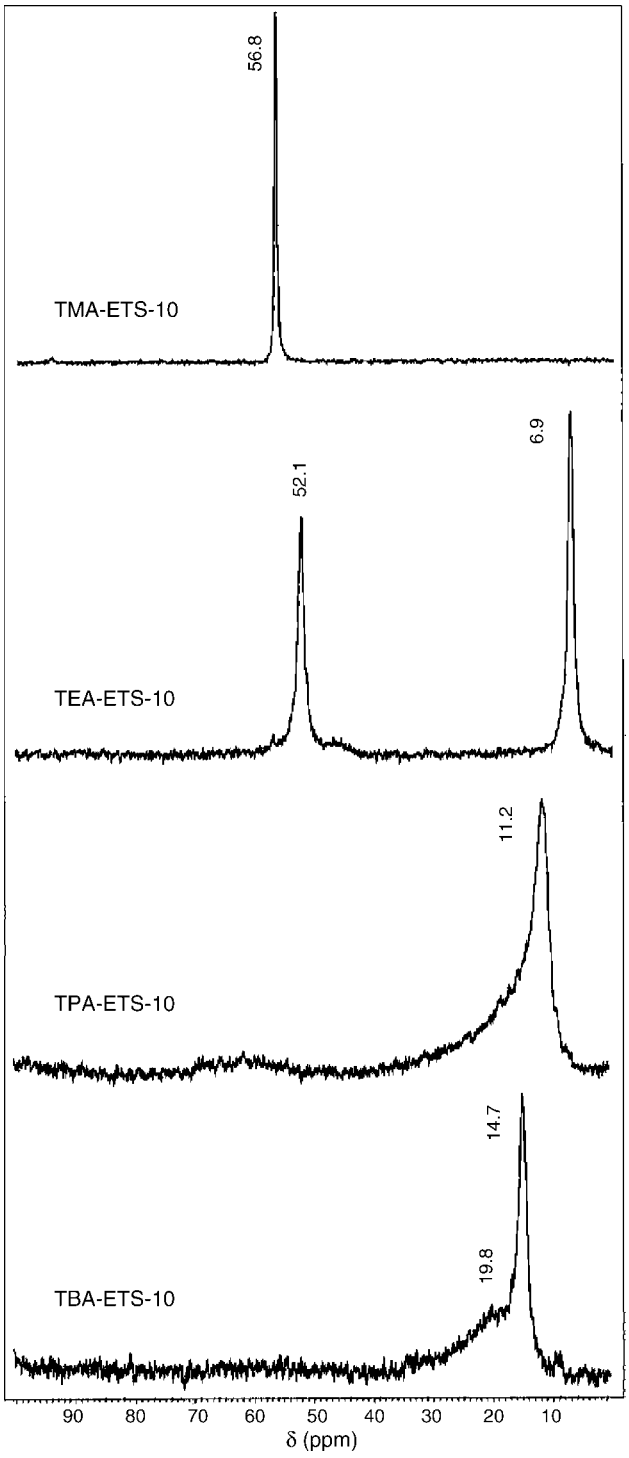

Fig. 8. ^{13}C NMR spectra of TAA-ETS-10 crystalls obtained at $190 \pm 2\,^{\circ}C$ for 72 h.

The DSC curves of ETS-10 (Fig. 7a) present one single endothermal peak corresponding to water elimination, with a maximum at $\sim 173\,^{\circ}C$ for initial co gel and $\sim 132\,^{\circ}C$ for ETS-10 with 100% crystallinity. The amorphous solids—initial and after 12 h present another endothermic peak at $\sim 622\,^{\circ}C$, which corresponds to melting and recrystallization of titanosilicate phase. The DSC patterns of TAA-ETS-10 solids (Fig. 7 b–e) shows an endothermic peak corresponding to water removal and another exothermic one as a result of overlapped melting, decomposition and combustion heat effects. The TAA salts are present in initial amorphous co gel, than TEA, TPA and TBA are absent after 12 h of heating at $190 \pm 2\,^{\circ}C$ and, once the crystallization takes place, the organic molecules are present in the structure of ETS-10 titanosilicate. The maximum of DSC peaks is $\sim 373\,^{\circ}C$ for TMA^+, $\sim 409\,^{\circ}C$ for TEA^+ and TPA^+ and $\sim 393\,^{\circ}C$ for TBA^+. The width of the peak decreases from TMA-ETS-10 to TBA-ETS-10 suggesting some difference in removal of the organic species based on the difference between the size of TAA molecule and of ETS-10 channel. Especially, the TPA^+ and TBA^+ cations are too large to diffuse out of the channels and must be decomposed into smaller molecules at elevated temperatures. It seems that only TMA^+ cations influence the nucleation stage and TEA^+, TPA^+ and TBA^+ cations have a retarding action.

The presence of the organic TAA cations into ETS-10 channels before calcinations were performed by ^{13}C NMR spectra and are present in Fig. 8.

The values of the chemical shifts from the ^{13}C NMR spectra of TAA-ETS-10 samples are quite close with the values of the corresponding TAA^+ ions in their hydrated form [52–54]. The ^{13}C NMR spectra of TAA-ETS-10 samples show only signals which originate from the A (alkyl) groups of the TAA^+ ions and the chemical shifts appear during their incorporation into the structure [35].

4. Conclusions

The results above reported show that the TAA^+ cations in the alkaline silica–titania co gel modify the nucleation time, the crystal growth rate and the morphology of ETS-10 crystals. The shorter alkyl chains of TMA^+ cations lead to more polar and relatively hydrophilic behavior, while the TEA^+, TPA^+ and TBA^+ cations are increasing in hydrophobicity.

A fast nucleation rate was observed for TMA^+ cation because of the agreement between the size of hydrated TMA^+ and the size of ETS-10 channels. This suggests that the presence of TMA^+ cations affects more the time necessary to reach the supersaturation threshold for ETS-10 nucleation.

TAA^+ cations present in the initial co gel influence the crystallization kinetic probably due to a modification of the solubility of reactive species and to the “structure-breaking” effect of TAA^+ cations on water; with increasing of TAA^+ size the cation–anion interactions are not so extensive and the cations have a retarding influence.

During the crystallization process the TAA^+ cations transit from the liquid phase into solid amorphous phase and finally are entrapped intact into the channels in their hydrated forms. The presence of TAA^+ in the crystalline voids of ETS-10 was confirmed by TG–TGD–DSC and ^{13}C NMR analysis.

The role of the TAA^+ cations in the synthesis process is as a "pore filling" rather than as a specific "structure-directing"; the synthesis of ETS-10 does not necessarily require the presence of TAA^+ cations. Nevertheless, the use of TAA salts as organic additives can be particularly useful when it is desired to modify crystallinity, the size and morphology of the crystals.

Acknowledgement

C.C. Pavel acknowledges Professor Alfonso Nastro for the postdoctoral stage in his laboratory of Technology and Applied Chemistry, University of Calabria (Cs) Italy.

References

[1] D.W. Breck, Zeolite Molecular Sieves: Structure, Chemistry and Use, John Wiley, New York, 1974.
[2] S.L. Burkett, M.E. Davis, Chem. Mater. 7 (1995) 920;
S.L. Burkett, M.E. Davis, Chem. Mater. 7 (1995) 1453.
[3] A. Corma, Chem. Rev. 97 (1997) 2373.
[4] W.O. Haag, Stud. Surf. Sci. Catal. 84 (1994) 1375.
[5] D.J. Parrillo, C. Pereira, G.T. Kokotailo, R.J. Gorte, Catalysis 138 (1992) 337.
[6] M.E. Davis, Microporous Mesoporous Mater. 21 (1998) 173.
[7] S.L. Burkett, M.E. Davis, J. Phys. Chem. 98 (1994) 9647.
[8] R. Szostak, Molecular sieves, in: Principles of Synthesis and Identification, van Nostrand Reinhold, New York, 1989, p. 190.
[9] G.T. Kerr, J. Phys. Chem. 70 (1966) 1047.
[10] R.W. Thompson, Molecular sieves, science and technology, in: H.G. Karge, J. Weitkamp (Eds.), Synthesis, vol. I, Springer-Verlag, Berlin, 1998, p. 1.
[11] R. van Grieken, J.L. Sotelo, J.M. Menendez, J.A. Melero, Microporous Mesoporous Mater. 39 (2000) 135.
[12] R.M. Barrer, P.J. Denny, J. Chem. Soc. (1961) 971.
[13] R. Aiello, R.M. Barrer, J. Chem. Soc. (A) (1970) 1470.
[14] M.E. Davis, S.I. Zones, in: L. Mario Occelli, Henry Kessler (Eds.), Synthesis of Porous Materials. Zeolites, Clays and Nanostructures, Marcel Dekker Inc., 1997, p. 1.
[15] S.M. Kuznicki, US Pat. 4,853,202 (1989).
[16] M.W. Anderson, O. Terasaki, T. Ohsuna, A. Philippou, S.P. MacKay, A. Ferreira, J. Rocha, S. Lidin, Nature 367 (1994) 347.
[17] M.W. Anderson, O. Terasaki, T. Ohsuna, P.J.O. Malley, A. Philippou, S.P. MacKay, A. Ferreira, J. Rocha, S. Lidin, Philos. Mag. B 71 (1995) 813.
[18] G. Cruciani, P. De Luca, A. Nastro, P. Pattison, Microporous Mesoporous Mater. 21 (1998) 143.
[19] X. Wang, A.J. Jacobson, Chem. Commun. (1999) 973.
[20] J. Rocha, A. Ferreira, Z. Lin, M.W. Anderson, Microporous Mesoporous Mater. 23 (1998) 253.
[21] H. Xu, Y. Zhang, A. Navrotsky, Microporous Mesoporous Mater. 47 (2001) 285.
[22] L. Lv, F. Su, X.S. Zhao, Microporous Mesoporous Mater. 76 (2004) 113.
[23] A. Nastro, D.T. Hayhurst, S.M. Kuznicki, Stud. Surf. Sci. Catal. 98 (1995) 22.
[24] T. Kr. Das, A.J. Chandwadkar, S. Sivasanker, Chem. Commun. (1996) 1105.
[25] C.C. Pavel, D. Vuono, L. Cantazaro, P. De Luca, N. Bilba, A. Nastro, J. B.Nagy, Microporous Mesoporous Mater. 56 (2002) 227.
[26] X. Yang, J.P. Paillard, H.F.W.J. van Breukelen, H. Kessler, E. Duprey, Microporous Mesoporous Mater. 46 (2001) 1.
[27] X. Liu, J.K. Thomas, Chem. Commun. (1996) 1435.
[28] C.C. Pavel, I. Asaftei, G. Iofcea, P. De Luca, D. Vuono, J. B.Nagy, A. Nastro, N. Bilba, in: E. van Steen, L.H. Callanan, M. Claeys (Eds.), Full Proceedings of 14th International Zeolite Conference, Cape Town, South Africa, 25–30 April, 2004, p. 334 (Book of Abstracts); ISBN: 0-958-46636-x (CD-ROM), 1-920-01724-0.
[29] P. De Luca, A. Nastro, Stud. Surf. Sci. Catal. 105 (1997) 221.
[30] Z. Lin, J. Rocha, P. Brandao, A. Ferreira, A.P. Esculeas, J.D. Pedrosa de Jesus, A. Philippou, M.W. Anderson, J. Phys. Chem. 101 (1997) 7114.
[31] V.P. Valtcev, S. Mintova, Zeolites 14 (1994) 697.
[32] V.P. Valtcev, J. Chem. Soc., Chem. Commun. (1994) 730;
V.P. Valtcev, J. Chem. Soc., Chem. Commun. (1994) 261.
[33] T.P. Das, A.J. Chandwadkar, A.P. Budhkar, S. Sivasanker, Microporous Mater. 5 (1996) 401.
[34] W.J. Kim, S.D. Kim, H.S. Jung, D.T. Hayhurst, Microporous Mesoporous Mater. 56 (2002) 89.
[35] C.C. Pavel, J. B.Nagy, N. Bilba, A. Nastro, C. Perri, D. Vuono, P. De Luca, I.V. Asaftei, Microporous Mesoporous Mater. 71 (2004) 77.
[36] A. Nastro, Z. Gabelica, P. Bodart, J. B.Nagy, in: S. Kaliaguine, A. Mahay (Eds.), Catalysis on the Energy Scene, vol. 19, Elsevier, Amsterdam, 1984, p. 131.
[37] R. Thompson, Zeolites 12 (1992) 680.
[38] W.M. Hendricks, A.T. Bell, C.J. Radke, J. Phys. Chem. 95 (1991) 9513.
[39] J.P. Gilson, Zeolite microporous solids: synthesis, structure and reactivity, in: E.G. Derouane, F. Lemos, C. Naccache, F.R. Ribeiro (Eds.), NATO ASI Ser., vol. 352, Kluwer Academic Publishers, Dordrecht, 1992, p. 19.
[40] A.V. Mc Cormick, A.T. Bell, Catal. Rev. Sci. Eng. 31 (1989) 97.
[41] F. Crea, J. B.Nagy, A. Nastro, G. Giordano, R. Aiello, Thermochim. Acta 135 (1988) 353.
[42] G. Engelhardt, Z. Anorg. Allg. Chem. 465 (1980) 15;
G. Engelhardt, Z. Anorg. Allg. Chem. 484 (1982) 22;
G. Engelhardt, Z. Anorg. Allg. Chem. 494 (1982) 31;
G. Engelhardt, Z. Anorg. Allg. Chem. 509 (1984) 85;
G. Engelhardt, Z. Anorg. Allg. Chem. 521 (1985) 22.
[43] J. B.Nagy, I. Ivanova, R. Aiello, F. Crea, A. Nastro, F. Nesta, Zeolites 15 (1995) 421.
[44] R.A. Robinson, R.H. Stokes, Electrolite Solutions, second ed., The Butterworts, London, 1968, p. 577.
[45] H. Sadek, J. Electroanal. Chem. 144 (1983) 11.
[46] Q. Gao, O. Giraldo, W. Tong, S.L. Suib, Chem. Mater. 13 (2001) 778.
[47] K. Tanaki, Bull. Chem. Soc. Jpn. 47 (1974) 2764.
[48] E.R. Nightingale Jr., J. Phys. Chem. 63 (1959) 1381;
E.R. Nightingale Jr., J. Phys. Chem. 66 (1962) 894.
[49] T. Osakai, K. Ebina, J. Phys. Chem. B 102 (1998) 5691.
[50] P.S. Nikan, A.B. Nikumbh, J. Chem. Eng. Data 47 (2002) 400.
[51] N. Bilba, C.C. Pavel, I. Asaftei, A. Nastro, J. B.Nagy, C. Perri, D. Vuono, D. De Luca, Gh. Iofcea, in: E. van Steen, L.H. Callanan, M. Claeys (Eds.), Full Proceedings of 14th International Zeolite Conference, Cape Town, South Africa, 25-30 April, 2004, p. 180 (Book of Abstracts); ISBN: 0-958-46636-x (CD-ROM), 1-920-01724-0.
[52] J. B.Nagy, Z. Gabelica, E.G. Derouane, Zeolites 3 (1983) 43.
[53] N. Dewaele, Z. Gabelica, P. Bodart, J. B.Nagy, G. Giordano, E.G. Derouane, Stud. Surf. Sci. Catal. 37 (1988) 65.
[54] Q. Chen, J. B.Nagy, J. Fraissard, J.El. Hage – Al Asswad, Z. Gabelica, E.G. Derouane, R. Aiello, F. Crea, G. Giordano, A. Nastro, NATO ASI Series, Physics 221 (1999) 87.